A flowing plasma model to describe drift waves in a cylindrical helicon discharge

L. Chang, M. J. Hole, and C. S. Corr

Citation: Physics of Plasmas (1994-present) **18**, 042106 (2011); doi: 10.1063/1.3581045
View online: http://dx.doi.org/10.1063/1.3581045
View Table of Contents: http://scitation.aip.org/content/aip/journal/pop/18/4?ver=pdfcov
Published by the AIP Publishing

A flowing plasma model to describe drift waves in a cylindrical helicon discharge

L. Chang,[a] M. J. Hole, and C. S. Corr
Plasma Research Laboratory, Research School of Physics and Engineering, The Australian National University, Canberra ACT 0200, Australia

(Received 20 February 2011; accepted 30 March 2011; published online 29 April 2011)

A two-fluid model developed originally to describe wave oscillations in the vacuum arc centrifuge, a cylindrical, rapidly rotating, low temperature, and confined plasma column, is applied to interpret plasma oscillations in a RF generated linear magnetized plasma [WOMBAT (waves on magnetized beams and turbulence)], with similar density and field strength. Compared to typical centrifuge plasmas, WOMBAT plasmas have slower normalized rotation frequency, lower temperature, and lower axial velocity. Despite these differences, the two-fluid model provides a consistent description of the WOMBAT plasma configuration and yields qualitative agreement between measured and predicted wave oscillation frequencies with axial field strength. In addition, the radial profile of the density perturbation predicted by this model is consistent with the data. Parameter scans show that the dispersion curve is sensitive to the axial field strength and the electron temperature, and the dependence of oscillation frequency with electron temperature matches the experiment. These results consolidate earlier claims that the density and floating potential oscillations are a resistive drift mode, driven by the density gradient. To our knowledge, this is the first detailed physics model of flowing plasmas in the diffusion region away from the RF source. Possible extensions to the model, including temperature nonuniformity and magnetic field oscillations, are also discussed. © *2011 American Institute of Physics*. [doi:10.1063/1.3581045]

I. INTRODUCTION

Oscillations have been observed in the electric probe signals of many laboratory plasmas, including theta pinches,[1,2] magnetic mirrors,[3–5] Q machines,[6] vacuum arc centrifuge,[7] and helicon plasmas.[8–12] Theta pinches and magnetic mirrors behave vastly different from the latter because of their high beta and significant magnetic curvature, which result in highly different plasma and field geometry. In contrast, Q machine, plasma centrifuge, and helicon plasmas have low-beta and negligible magnetic curvature, and have similar plasma properties. We exploit this similarity by deploying a two-fluid collisional model, initially developed to describe vacuum arc centrifuge plasmas, to describe the configuration and oscillations in a helicon plasma. Our goal is to better describe a class of electrostatic oscillations observed, but not yet conclusively identified, in the diffusion region of helicon plasmas, away from the RF source.

The helicon plasma we study is provided by the WOMBAT (waves on magnetized beams and turbulence)[13] device, which was designed to provide a plasma environment to study wave physics, including chaos, turbulence, wave saturation, and the related driving mechanisms. WOMBAT has been used to study helicon waves,[10,14,15] which have attracted great interest in the past decades due to their ability to produce high plasma densities.[16] Such plasmas also provide a rich environment for the experimental study of drift waves and their impact on anomalous transport,[17] which is important to understand in fusion plasmas. Although there have been many publications on helicon wave physics, less attention has been devoted to the physics of low frequency oscillations in the diffusion region away from the source.[18] Light *et al.*[19,20] observed a low frequency electrostatic instability only above a critical magnetic field and identified it as a mixture of drift waves and a Kelvin–Helmholtz instability. Degeling *et al.*[10,21] observed relaxation oscillations in the kilohertz range that were associated with the various types of mode coupling in helicon discharges. More recently, a cylindrical linear model which treats global eigenmodes[22] has been employed to study drift waves in the magnetically confined plasma device VINETA (versatile instrument for studies on nonlinearity, electromagnetism, turbulence and applications),[17,18,23] however, the model does not involve the $\mathbf{E} \times \mathbf{B}$ rotation and neglects ion parallel motion which may influence the characteristics of low frequency oscillations.[24] Sun *et al.*[12] observed low frequency (13 kHz) oscillations near the end of helicon source region, and identified them as resistive-drift Alfvén waves. Sutherland *et al.*[25] observed low frequency ion cyclotron waves that were highly localized along the axial center of the WOMBAT plasma device. Spectral measurements revealed a four-wave interaction where energy is down-converted to the ion cyclotron mode from the helicon pump.

Low frequency oscillations in helicon plasmas can be broadly classified into two types: the Kelvin–Helmholtz instability and drift waves. The Kelvin–Helmholtz instability is driven by a velocity shear in a mass flow or a velocity difference across the interface between two fluids.[26] This can occur in helicon plasmas, because the streaming velocity of the ion fluid is much slower than that of electrons. The drift wave is a universal instability driven by a plasma pressure gradient perpendicular to the ambient field.[27] It can arise in

[a]Electronic mail: chang.lei@anu.edu.au.

fully ionized, magnetically confined, and low-beta plasmas,[28] and has been observed in both linear and toroidal field geometries.[29–33] In WOMBAT plasmas, the velocity shear is small, and the density and temperature gradients produce large pressure gradients, suggestive of large drive of drift waves. We thus restrict attention to this class of modes.

In this paper, a two-fluid model, which was developed originally for the vacuum arc centrifuge by Hole *et al.*[34,35] to explain oscillations observed in the density and electric potential, is applied to study low frequency oscillations observed in WOMBAT. We show that the equilibrium and perturbed density profiles and the space potential profile from the model and data are consistent. The model predicts unstable modes, with a similar global mode radial structure, and a frequency comparable to observed signals. The paper is organized as follows: Sec. II gives a brief description of the experimental setup (WOMBAT), Sec. III introduces the two-fluid model, and Sec. IV discusses the wave physics revealed by this model and the data. Finally, Sec. V discusses the possible extensions to this model and presents concluding remarks.

II. EXPERIMENTAL SETUP

A schematic[36] of the experiment is shown in Fig. 1. The WOMBAT experiment comprises a glass source tube and a large stainless steel diffusion chamber, which are attached to each other on axis. The source tube is 50 cm long and 18 cm in diameter, while the diffusion chamber is 200 cm long and 90 cm in inner diameter. A large solenoid is employed inside the diffusion chamber to provide a steady magnetic field, which can be up to 0.02 T and highly uniform along the axis. To generate the plasma, a single loop antenna (20 cm in diameter, 1 cm wide, and 0.3 cm thick) surrounding the source tube coupled RF power to the argon gas. The 7.2 MHz electric current passing through the loop creates a time varying magnetic field, which in turn induces azimuthal current in the argon gas, and leads to break down and formation of the plasma.[37] The base pressure of the diffusion chamber was maintained at 4×10^{-6} Torr by a turbomolecular pump and a rotary pump. In this work, the large solenoid was used to produce a high-density blue core in the diffusion chamber.

To measure spatial and temporal profiles in the plasma, an uncompensated, translating Langmuir probe was inserted radially into the diffusion chamber, 50 cm from the source and diffusion chamber interface. The central wire of the probe was fed through an alumina support which was in turn shielded by a 6 mm diameter grounded steel tubing covering the whole extent of the probe length up to the probe tips. The removable probe tip was made of a 0.2 mm diameter and 8 mm long nickel wire. Radial translation of the probe was set using a computer controlled stepper motor arrangement that allowed the probe tip position to be selected with an accuracy of a few micrometers. To determine the plasma $I(V)$ characteristics, the bias voltage on the Langmuir probe was swept between -50 and $+30$ V using a *Labview* program. The plasma density (n_i), electron temperature (T_e), plasma potential (V_p), and floating potential (V_f) were determined from the $I(V)$ characteristics of the cylindrical probe. For the present high-density plasma discharge, the effect that rf fluctuations have on the floating potential, and hence the $I(V)$ characteristics, was found to be negligible. The effect that fluctuations due to waves will have on time-averaged $I(V)$ characteristics will be far more dominant than the rf fluctuations. These wave fluctuations would lead to error magnification in the second derivative of the $I(V)$ curve and hence the electron energy distribution function. For this reason, the plasma parameters were obtained directly from the $I(V)$ curve and not by the Druyvesteyn method.[38]

Typical Langmuir probe measurements of WOMBAT argon plasmas are shown in Table I. Other parameters, obtained for similar helicon plasmas[39,40] and measured by laser induced fluorescence, include: the ion temperature T_i, the bulk rotation frequency ω_0, and axial streaming velocity V_{z0}. The parameter m_i is the argon ion mass, and the charge number Z is taken to match similar argon plasma conditions.[41] The remaining parameters are introduced in Sec. III. Finally, plasma parameters for the PCEN (plasma centrifuge) device are taken from published work.[34,42] It should be noted that the operating gas in the PCEN work is magnesium, while here it is argon.

III. PLASMA MODEL

A. Model assumptions

The two-fluid model developed by Hole *et al.*[34,43] is based on the following plasma assumptions:

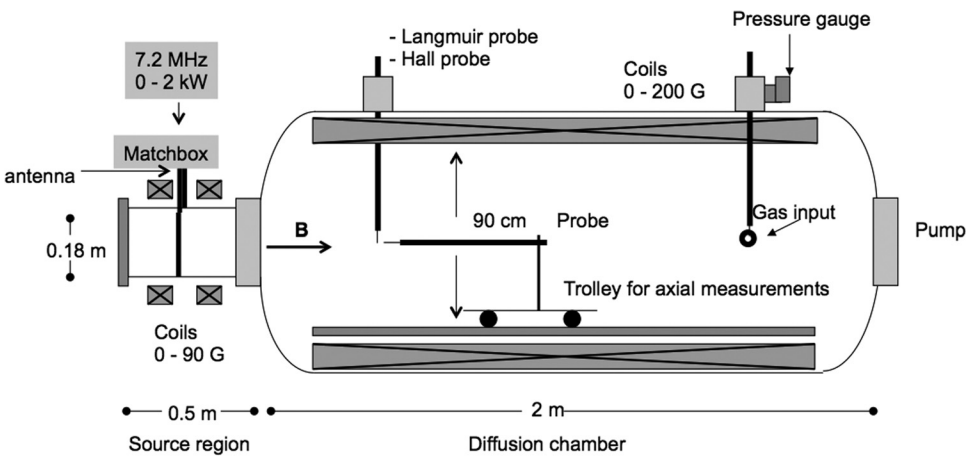

FIG. 1. A schematic of the WOMBAT (waves on magnetized beams and turbulence) plasma experiment.[36]

TABLE I. Typical parameters of WOMBAT and PCEN (plasma centrifuge).

Parameter	WOMBAT	PCEN (Refs. 34 and 42)
n_i (on axis)	1.4×10^{19} m^{-3}	5.2×10^{19} m^{-3}
T_e	1.5 eV	2.9 eV
T_i	0.1 eV	2.9 eV
m_i	40 amu (Ar)	24.31 amu (Mg)
B_z	0.0185 T	0.05 T
Z	1.0	1.5
V_{z0}	200 m s^{-1}	10^4 m s^{-1}
ω_0	1.42 krad s^{-1}	184 krad s^{-1}
$\omega_{ic} = \frac{B_z eZ}{m_i}$	44.5 krad s^{-1}	295 krad s^{-1}
$\Omega_{i0} = \frac{\omega_0}{\omega_{ic}}$	0.032	0.59
$\Psi = \left(\frac{T_i}{T_e} + Z\right) \frac{k_B T_e}{m_i \omega_{ic}^2 R^2}$	0.54	1.6
$\delta = \frac{eZn_{i0}}{B_z} \frac{\eta_L}{\gamma_E}$	0.0235	0.03
R (characteristic radius)	6 cm	1.43 cm

1. Ions of different charge can be treated as a single species with average charge Z.
2. The plasma is quasineutral, giving that $n_e = Zn_i$
3. The steady-state plasma is azimuthally symmetric and has no axial structure.
4. The effects induced by plasma fluctuations on the externally applied field can be neglected.
5. Both finite Larmor radius (FLR) and viscosity effects are negligible.
6. For the range of frequencies considered here, the electron inertia can be neglected.
7. The ion and electron temperatures, T_i and T_e, are uniform across the plasma column.
8. The steady-state ion density distribution has a form of $n_0 = n_i(0)e^{-(r/R)^2}$, which is a Gaussian profile. Here, $n_i(0)$ is the on-axis ion density, and R is the characteristic radius at which the density is $1/e$ of its on-axis value.
9. The steady-state velocities of ions and electrons can be written as $\mathbf{v_i} = (0, \omega_i r, v_{iz})$ and $\mathbf{v_e} = (0, \omega_e(r)r, v_{ez}(r))$, respectively, where ω_i is the ion rigid rotor rotation frequency, v_{iz} is the ion uniform axial streaming velocity, $\omega_e(r)$ is the electron rotation frequency, and $v_{ez}(r)$ is the electron streaming velocity. While treated in other work,[43] radial diffusion of both ions and electrons due to electron–ion collision is negligible.

Here, length and time are normalized to R and $1/\omega_{ic}$, respectively, where $\omega_{ic} = ZeB_z/m_i$ is the ion cyclotron frequency. A cylindrical coordinate system is developed, with $(x, \theta, \varsigma) = (r/R, \theta, z/R)$ and $\tau = \omega_{ic}t$, where x and ς are the normalized radial and axial positions, respectively.

B. Two-fluid equations

The model comprises the motion and continuity equations of ion and electron fluids written, respectively, as

$$\frac{\partial \mathbf{u_i}}{\partial \tau} + (\mathbf{u_i} \cdot \nabla)\mathbf{u_i} = -\psi(Z\nabla\chi + \lambda\nabla l_i) + \mathbf{u_i} \times \hat{\varsigma} + \delta \mathrm{n_s} \tilde{\xi} \cdot (\mathbf{u_e} - \mathbf{u_i}), \tag{1}$$

$$\psi Z(-\nabla l_i + \nabla\chi) - \mathbf{u_e} \times \hat{\varsigma} + \delta \mathrm{n_s} \tilde{\xi} \cdot (\mathbf{u_i} - \mathbf{u_e}) = 0, \tag{2}$$

$$-\frac{\partial l_i}{\partial \tau} = \nabla \cdot \mathbf{u_i} + \mathbf{u_i} \cdot \nabla \mathrm{l_i}, \tag{3}$$

$$-\frac{\partial l_i}{\partial \tau} = \nabla \cdot \mathbf{u_e} + \mathbf{u_e} \cdot \nabla \mathrm{l_i}, \tag{4}$$

with terms defined as follows:

$$\mathbf{u_i} = \frac{\mathbf{v_i}}{\omega_{ic}\mathrm{R}} = (\mathrm{x}\varphi_\mathrm{i}, \mathrm{x}\Omega_\mathrm{i}, \mathrm{u_{i\varsigma}}), \mathbf{u_e} = \frac{\mathbf{v_e}}{\omega_{ic}\mathrm{R}} = (\mathrm{x}\varphi_\mathrm{e}, \mathrm{x}\Omega_\mathrm{e}, \mathrm{u_{e\varsigma}}),$$

$$\lambda = \frac{T_i}{T_e}, \psi = \frac{k_B T_e}{m_i \omega_{ic}^2 R^2}, \chi = \frac{e\phi}{k_B T_e}, \tilde{\xi} = diag(\xi_\perp, \xi_\perp, 1),$$

$$l_i = ln\frac{n_i}{n_i(0)}, n_s = \frac{\nu_{ei}}{\nu_{ei}(0)}, \delta = \frac{eZn_{i0}}{B_z}\frac{\eta_L}{\gamma_E}.$$

Here, subscripts i and e refer to ion and electron parameters, respectively, φ is the normalized radial velocity divided by x, Ω is the normalized rotation frequency, u_ς indicates the normalized axial velocity, λ is the ratio between ion and electron temperatures, ψ is a convenient constant which for $\lambda = 1$ becomes the square of the normalized ion thermal velocity, χ is a normalized electric potential ϕ, l_i is the logarithm of the ratio of the ion density n_i to its on-axis value $n_i(0)$, and n_s is the ratio of the electron–ion collision frequency ν_{ei} to its on-axis value $\nu_{ei}(0)$. Also, δ is the normalized resistivity parallel to the magnetic field, where η_L is the electrical resistivity of a Lorentz gas and γ_E is the ratio of the conductivity of a charge state Z to that in a Lorentz gas.[44]

C. Steady-state solution

In cylindrical geometry with a purely axial constant field $\mathbf{B} = (0, 0, B_z)$, the steady-state solution of this model is given by

$$\chi_0(x) = \chi_c + \left[\frac{\Omega_{i0}}{2\psi Z}(1 + \Omega_{i0}) + \frac{\lambda}{Z}\right]x^2, \tag{5}$$

with

$$\Omega_{e0} = \Omega_{i0}(1 + \Omega_{i0}) + 2\psi(\lambda + Z), \tag{6}$$

where χ_c is an arbitrary reference potential. The axial current in this model is unconstrained, and can arbitrarily be set to zero ($u_{i\varsigma 0} = u_{e\varsigma 0}$), consistent with WOMBAT boundary conditions.

We have compared the steady-state solution to experimental data. Measurements of the fluctuation frequency from probe measurements suggest rigid rotation, which is consistent with the spectroscopic data obtained by Scime *et al.*[40] Figure 2(a) shows the equilibrium density profile of the WOMBAT plasma for two different axial field strengths, $B_z = 0.0185$ T and $B_z = 0.0034$ T, respectively.[15] Overlaid are best fits to the profile using a Gaussian profile ($n_{i0} = n_i(0)e^{-(r/R)^2}$): these show reasonable agreement over the range of the data. The stronger field produces better confinement with a smaller characteristic radius R.

Figure 2(b) shows the radial variation of the space potential in WOMBAT for a slightly different field strength, $B_z = 0.0068$ T.[36] Overlaid is a best fit to the data using the

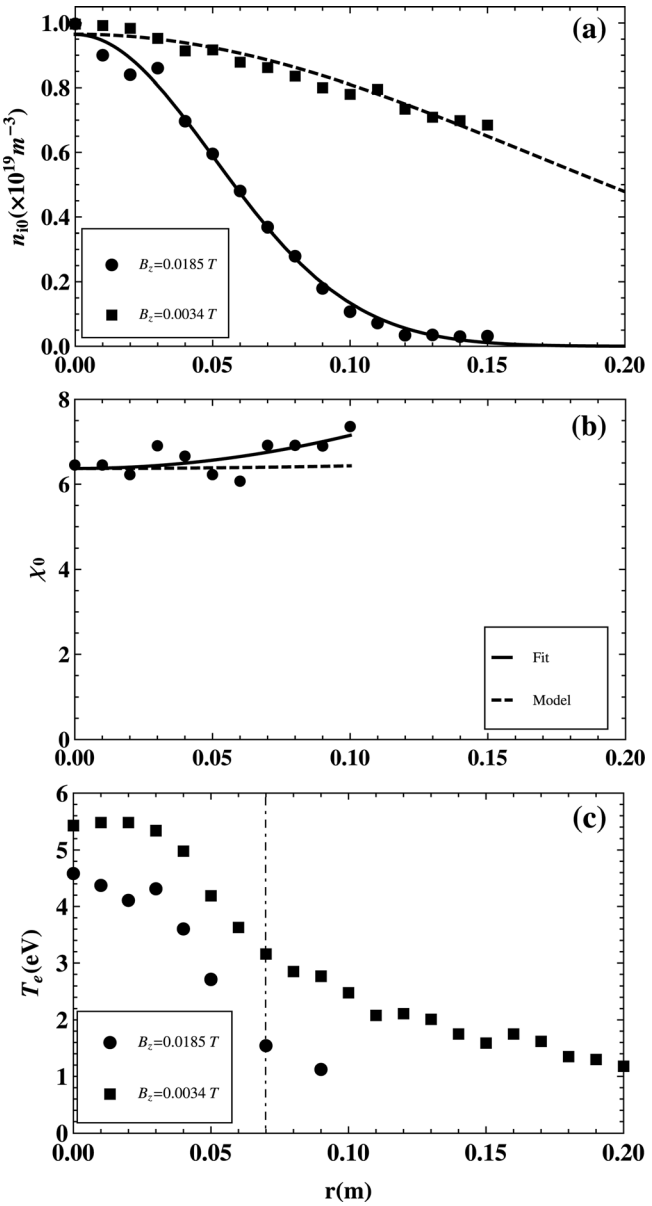

FIG. 2. Plasma configuration of WOMBAT: (a) Gaussian fit of the equilibrium density profile, for $B_z = 0.0185$ T and $B_z = 0.0034$ T, respectively[15]; (b) the radial variation of the normalized space potential from the fit procedure (solid line), the model (dashed), and the data (dots),[36] which was taken under the conditions of $B_z = 0.0068$ T, 0.6 mTorr, and 1708 W in the experiment; (c) the radial profile of the electron temperature at two field strengths: $B_z = 0.0185$ T and $B_z = 0.0034$ T.[15] The dashed vertical line in (c) corresponds to the radial location of fluctuation measurements.

parabolic potential profile in Eq. (5), with the arbitrary reference potential (χ_c) and gradient $G = \frac{\Omega_{i0}}{2\psi Z}(1 + \Omega_{i0}) + \frac{\lambda}{Z}$ free parameters. Although the fit, for which $G = 0.5$, is reasonable, the scatter in the data is large. For the same χ_c, we have over plotted the model potential profile with $G = 0.04$. Within the bulk of the plasma, out to the characteristic radius $r = 0.08$ m, model and observed potential profiles broadly agree.

Figure 2(c) shows the radial profile of T_e in the WOMBAT plasma.[15] The constant electron temperature of the model is an approximation to the radially varying experimental profile. For the model, we have chosen the T_e value at the position at which the frequency was determined, $r = 7$ cm.

D. Normal mode analysis

To compute the normal modes of the system, Hole *et al.*[34] apply a linear perturbation treatment with plasma parameters ζ taking the form

$$\zeta(\tau, x, \theta, \varsigma) = \zeta_0(x) + \varepsilon\zeta_1(x)e^{i(m\theta + k_\varsigma \varsigma - \omega\tau)}. \tag{7}$$

Here, ε is the perturbation parameter, m the azimuthal mode number, k_ς the axial wave number, and ω the angular frequency. To first order in ε the system of Eqs. (1)–(4) reduces to

$$\begin{pmatrix} \psi(l_{i1}'(y) - X_1'(y)) \\ y\varphi_{i1}'(y) \\ y\varphi_{e1}'(y) - im\Psi X_1'(y) \\ \Psi\delta\xi_\perp e^{-y} X_1'(y) \\ 0 \end{pmatrix} = \widetilde{\mathbf{A}} \begin{pmatrix} l_{i1}(y) \\ X_1(y) \\ \varphi_{i1}(y) \\ \varphi_{e1}(y) \\ u_{e\varsigma}(y) \end{pmatrix}, \tag{8}$$

where $\widetilde{\mathbf{A}}$ is the matrix

$$\widetilde{\mathbf{A}} = \begin{pmatrix} \frac{m\Psi C}{2\bar{\omega}y} & 0 & \frac{i\bar{\omega}}{2} - \frac{iC^2}{2\bar{\omega}} & \frac{iC}{2\bar{\omega}} & 0 \\ \frac{i}{2}\left(\bar{\omega} - \frac{\Psi}{\bar{\omega}}\left(\frac{m^2}{y} + k_\varsigma^2\right)\right) & 0 & -1 + y - \frac{mC}{2\bar{\omega}} & \frac{m}{2\bar{\omega}} & 0 \\ \frac{i}{2}(\bar{\omega} - m\Omega_{i0}^2 - 2m\Psi) & 0 & 0 & -1 + y & -\frac{ik_\varsigma}{2} \\ 0 & \frac{im\Psi}{2y} & 0 & -\frac{1}{2} & 0 \\ 0 & -ik_\varsigma\Psi & 0 & 0 & 0 \end{pmatrix} + \delta \begin{pmatrix} 0 & 0 & -\frac{\xi_\perp e^{-y}}{2} & \frac{\xi_\perp e^{-y}}{2} & 0 \\ 0 & 0 & 0 & 0 & 0 \\ 0 & 0 & -\frac{im\xi_\perp e^{-y}}{2} & \frac{im\xi_\perp e^{-y}}{2} & 0 \\ \xi_\perp e^{-y}\left(-\frac{m\Psi}{2\bar{\omega}y} + \frac{\Omega_{i0}^2}{2} + \Psi\right) & 0 & \frac{iC\xi_\perp e^{-y}}{2\bar{\omega}} & -\frac{i\xi_\perp e^{-y}}{2\bar{\omega}} & 0 \\ \frac{e^{-y}k_\varsigma\Psi}{\bar{\omega}} & 0 & 0 & 0 & -e^{-y} \end{pmatrix}. \tag{9}$$

Here, $\bar{\omega} = \omega - m\Omega_{i0} - k_\varsigma u_{\varsigma 0}$ is the frequency in the frame of the ion fluid, $C = 1 + 2\Omega_{i0}$, $\Psi = (\lambda + Z)\psi$, $y = x^2$, and we have introduced a new dependent variable $X_1(y)$, where

$$X_1(y) = \frac{Z}{Z + \lambda}[l_{i1}(y) - \chi_1(y)]. \tag{10}$$

For large axial wavelength modes of the resistive plasma column, for which $k_\varsigma^2 \le \delta$, this model can be reduced to a second order differential equation

$$\left(\frac{\bar{\omega}^2 - C^2}{\bar{\omega}\Psi}\right) L(N_c)[g_1(y)] = 0, \tag{11}$$

where

$$L(N_c) = y\frac{\partial^2}{\partial y^2} + (1 - y)\frac{\partial}{\partial y} + \left(\frac{N_c}{2} - \frac{m^2}{4y}\right),$$

$$N_c = \frac{(\bar{\omega}^2 - C^2)\left(m + \frac{i}{2}f(y)\right)}{\bar{\omega} - m\Omega_{i0}^2 + i\Psi f(y)} + \frac{mC}{\bar{\omega}},$$

and $f(y) = F^2 e^y$ with the normalized axial wave number $F = k_\varsigma/\sqrt{\delta}$. For odd m modes, the boundary conditions for

Eq. (11) are $g_1(0) = 0$ and $g_1(Y) = 0$ with the infinite radius Y representing the edge of plasma column. For even m, these conditions become $g_1'(0) = 0$ and $g_1(Y) = 0$. We seek unstable solutions to Eq. (11), for which $\bar{\omega}^i > 0$. The solutions $\bar{\omega} = \pm C$ are stable and hence discarded.

IV. WAVE PHYSICS

The experimental results indicate that a $m = 1$ drift wave mode dominates the density fluctuations, and that the mode appears to propagate purely azimuthally in direction of the electron diamagnetic drift.[45] There is no clear radial component of the mode propagation. The observed phase velocity of the mode is approximately 200 m/s in the region of maximum density perturbation.

A. Dispersion curve

As in Hole *et al.*[34] we have solved Eq. (11) by a shooting method. For $m = 1$ the boundary conditions are $g_1(0) = g_1(Y) = 0$. As the differential equation is homogeneous, the gradient at the edge $g_1'(Y)$ is arbitrary: we have chosen $g_1'(Y) = 1$. To solve for given F, we choose a trial $\bar{\omega}$ and march the solution from the edge to the core. The complex frequency $\bar{\omega}$ is then adjusted until the on-axis boundary condition is satisfied. We commence the procedure at $F = 0$, for which an analytical solution for $\bar{\omega}$ is available. This is found from the solution to

$$N_c = \frac{m(\bar{\omega}^2 - C^2)}{\bar{\omega} - m\Omega_{i0}^2} + \frac{mC}{\bar{\omega}} = 2n + |m|, \qquad (12)$$

where n is the number of radial nodes in the plasma.

Figure 3 shows the dispersion curve for the plasma conditions of the PCEN in Table I. We have compared the dispersion curve to Hole *et al.*[34] and found it to be identical, thus validating our numerics. For PCEN plasmas, the peak of normalized growth rate $\bar{\omega}^i = 0.39$ lies at $F = 0.3$, with normalized frequency $\bar{\omega}^r = 0.007$: the wave is thus near stationary in the frame of the ion fluid. The mode crossings located at $F = 0.55$ are associated with the centrifugal instability. Also shown is the dispersion curve for WOMBAT plasma conditions of Table I. For WOMBAT plasmas, the peak growth rate of $\bar{\omega}^i = 0.14$ occurs at $F = 0.37$, for which $\bar{\omega}^r = 0.44$. There is no mode crossing in the dispersion curve for WOMBAT plasmas. Also, $\bar{\omega}^r > 0$, and so in the laboratory frame $\omega^r = \bar{\omega}^r + m\Omega_{i0} + k_\varsigma u_{\varsigma 0}$, approximately $\omega^r \approx \bar{\omega}^r + \Omega_{i0}$, such that the frequency of unstable waves is always larger than the sum of the plasma rotation frequency and axial velocity, and the wave propagates in the $+\theta$ direction (electron diamagnetic drift direction). We attribute the difference between dispersion curves to the very low ion temperature T_i and slow normalized rotation frequency Ω_{i0} in WOMBAT plasmas, compared with PCEN plasmas. Indeed, this can be seen by varying the parameters from PCEN to WOMBAT conditions. If Ψ is held fixed and Ω_{i0} lowered, the growth rate drops linearly with Ω_{i0}, and the dispersion curve shifts to lower k_ς. Conversely, if Ω_{i0} is held fixed and Ψ lowered, the dispersion curve expands to higher k_ς, and the growth rate drops. Thus, the decrease in growth rate is due to both the decrease in rotation and temperature, while the expansion of the dispersion curve to higher k_ς is due to the lower temperature. The corresponding increase in $\bar{\omega}^r$ at low k_ς occurs because as rotation drops, the Doppler shifted frequency, $\bar{\omega}^r = \omega^r - m\Omega_{i0} - k_\varsigma u_{\varsigma 0}$, increases.

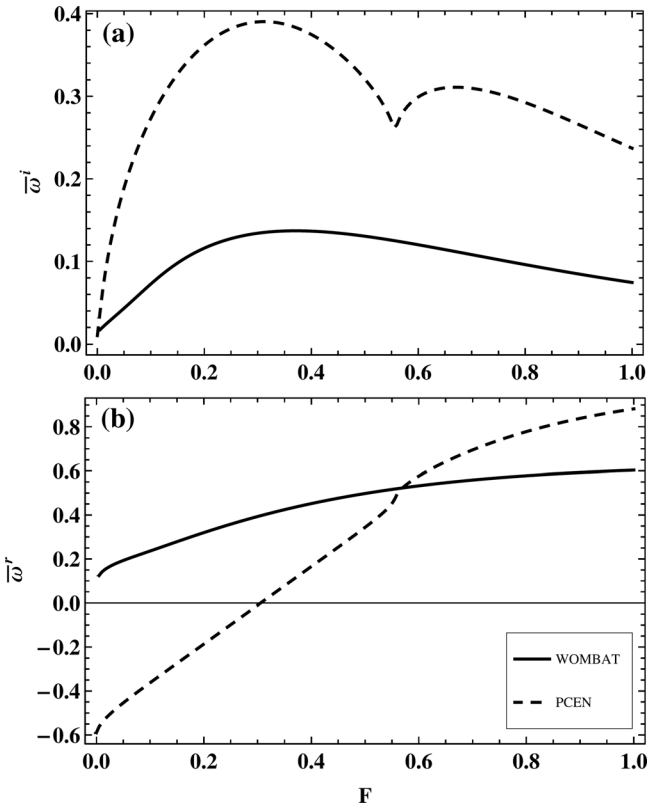

FIG. 3. Dispersion curves of PCEN (dashed line) and WOMBAT (solid line), generated by the model based on the conditions shown in Table I: (a) normalized growth rate $\bar{\omega}^i$; (b) normalized frequency $\bar{\omega}^r$. (vs normalized axial wave number $F = k_\varsigma/\sqrt{\delta}$.)

B. Dispersion curve sensitivity with plasma parameters

We have examined the sensitivity of the WOMBAT plasma dispersion curve with Ω_{i0}, B_z, and T_e. For $\Omega_{i0} < 0.05$ the dispersion curve changes by less than 1%. Figure 4 shows the change in dispersion curve for different B_z and T_e. Figures 4(a) and 4(b) shows that $\bar{\omega}^i$ and $\bar{\omega}^r$ decrease with increasing B_z: the physical growth rate $\omega^i = \bar{\omega}^i \omega_{ic}$ also obeys this trend while $\omega^r = \bar{\omega}^r \omega_{ic}$ exhibits the same trend in the range $F > 0.5$. Also, the peak growth rate shifts to lower k_ς, and so for constant R the axial wavelength of the most unstable mode is increased. In contrast, Figs. 4(c) and 4(d) shows that $\bar{\omega}^i$ and $\bar{\omega}^r$ increase with increasing T_e, and the peak growth rate shifts to larger k_ς. The dependence of growth rate with pressure gradient, and frequency with inverse field strength is consistent with a resistive drift wave.[27]

C. Wave oscillation frequency with B_z and T_e

In this section we compute the variation in wave frequency at the maximum growth rate with field strength, for two choices of electron temperature: a constant $T_e = 2.13$

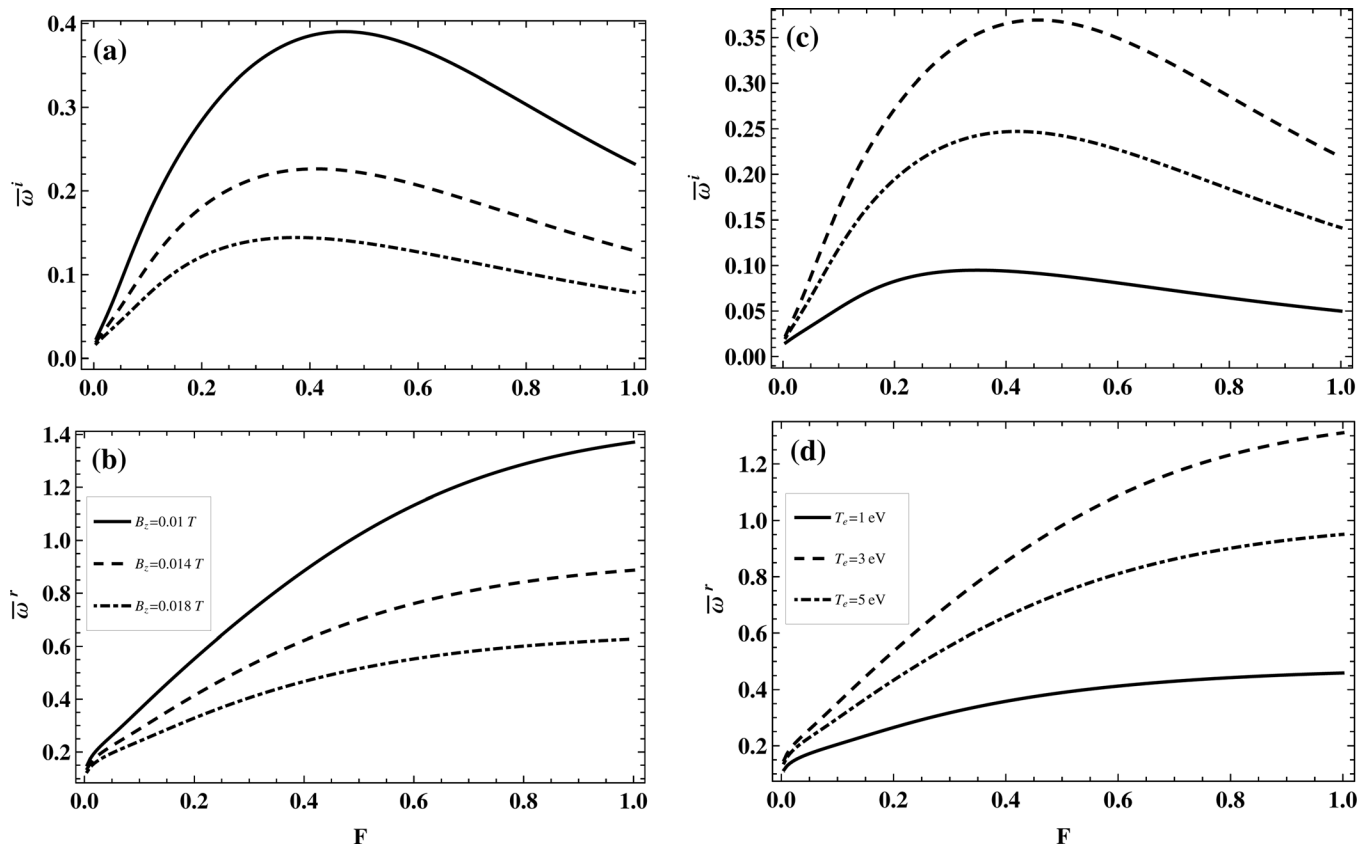

FIG. 4. Results of dispersion curve sensitivity with B_z and T_e: (a), (b) scanning results of B_z; (c), (d) scanning results of T_e.

eV, independent of B_z; and a B_z dependent T_e. As T_e data are only available at two field strengths [Fig. 2(c)]: $B_z = 0.0185$ T, $T_e = 3.2$ eV; and $B_z = 0.0034$ T, $T_e = 1.5$ eV, we have used linear interpolation to compute T_e at other field strengths. Fluctuation data are available at five field strengths: $B_z = 0.0129$ T, $B_z = 0.0146$ T, $B_z = 0.0162$ T, $B_z = 0.0179$ T, and $B_z = 0.0195$ T. We have solved the dispersion curve for each case, and selected $\bar{\omega}^r$ corresponding to the maximum $\bar{\omega}^i$ to calculate the frequency in the laboratory frame.

Figure 5 shows the measured and predicted oscillation frequencies. For both curves, the predicted and measured frequencies differ by a factor of 3.5. There are various possible reasons for this gap. The most likely is that the model assumes flat T_e and T_i profiles, whereas WOMBAT plasmas exhibit a nonuniform T_e profile. It may also be the case that the T_i profile is nonuniform. Second, there may be slip between the rotation of WOMBAT plasmas and the oscillation frequency. Third, we have neglected the fluctuations in the magnetic field, which may affect the dispersion curve. Finally, the calculation of T_e for each B_z is a linear interpretation between the two known data, which may bring errors and imprecisions into the prediction.

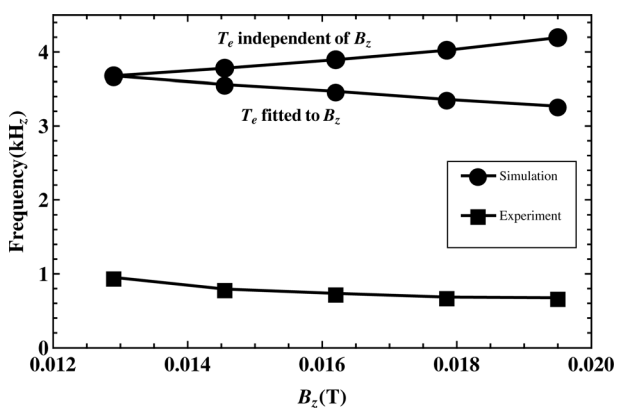

FIG. 5. Wave oscillation frequency with B_z and T_e.

Figure 5 also reveals that two trends predicted by using a constant $T_e = 2.13$ eV and a B_z dependent T_e are divergent. Predictions for the B_z dependent T_e profile exhibit the same trend as the data, suggesting the model may have correctly captured the T_e dependence with B_z.

Finally, to ensure that this model is in principle capable to reproduce the data, we adjusted T_e to fit the data points. We found that a value of $T_e = 0.5$ eV at low field dropping to $T_e = 0.3$ eV at high field was able to reproduce the observed frequency.

D. Perturbed density profile

Figure 6 shows the measured and predicted radial profiles of the perturbed density n_{i1}, together with the equilibrium density gradient $|n'_{i0}(r)|$. The data used here were taken under the conditions of $B_z = 0.01$ T, $R = 7.6$ cm, and $T_e = 2.46$ eV. The linear perturbation treatment gives no solution for the absolute magnitude of n_{i1}, and so we have fitted for the amplitude. Inspection of Fig. 6 suggests n_{i1} has a single peak, and therefore consistent with $n = 0$ of the perturbed mode. Also, the peak of the eigenfunction occurs in

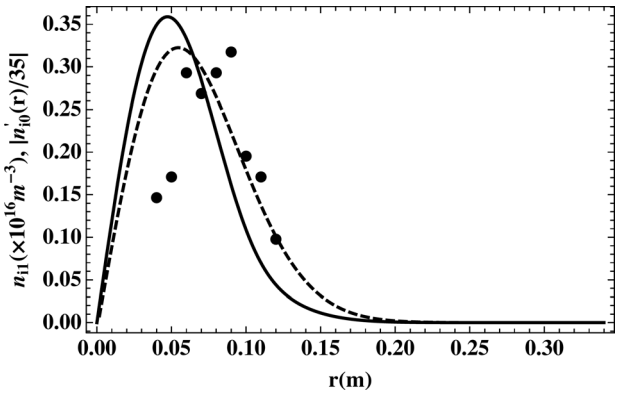

FIG. 6. Comparison between the measured (dots) and predicted (solid line) radial profiles of the perturbed density n_{i1}, together with the equilibrium density gradient $|n\prime_{i0}(r)|$ (dashed line).

the region where the equilibrium density gradient is large, suggesting that the instability has resistive drift-type characteristics.[28] The exact radial position of the peak in n_{i1}, however, does not agree. This could be due to uncertainty in the core position of the plasma or the assumption of constant T_e in the model.

Finally, to complement our visualization of the mode structure, we have computed the vector field of the linear perturbed mass flow by $m_i(n_{i1}\mathbf{u_{i0}} + n_{i0}\mathbf{u_{i1}})$. The perturbed velocity components $\mathbf{u}_{i1} = (\mathrm{x}\varphi_{\mathrm{i1}}, \mathrm{x}\Omega_{\mathrm{i1}}, \mathrm{u}_{\mathrm{i}\varsigma 1})$, $\mathbf{u}_{e1} = (\mathrm{x}\varphi_{\mathrm{e1}}, \mathrm{x}\Omega_{\mathrm{e1}}, \mathrm{u}_{\mathrm{e}\varsigma 1})$ and perturbed density n_{i1} can be computed from the solution of $g_1(y)$ and following equations:

$$l_{i1}(y) = \frac{-g_1(y)}{\left(1 + \frac{i}{\Psi}\left(\frac{m\Omega_{i0}^2 + 2m\Psi - \bar{\omega}}{f(y) - 2im}\right)\right)}, \tag{13}$$

$$\chi_1(y) = -\frac{\lambda}{Z} l_{i1}(y) - \left(1 + \frac{\lambda}{Z}\right) g_1(y), \tag{14}$$

$$\varphi_{i1}(y) = \frac{2\bar{\omega}}{i(\bar{\omega}^2 - C^2) - \bar{\omega}\delta\xi_\perp e^{-y}} [\Psi(l_{i1}\prime(y) - X_1\prime(y)) - \frac{m\Psi C}{2\bar{\omega}y} l_{i1}(y) - \left(\frac{iC}{2\bar{\omega}} + \frac{\delta\xi_\perp e^{-y}}{2}\right)\varphi_{e1}(y)\Big], \tag{15}$$

$$\varphi_{e1}(y) = \frac{2\bar{\omega}}{\bar{\omega} + i\delta\xi_\perp e^{-y}} \Big[\frac{im\Psi}{2y} X_1(y) - \Psi\delta\xi_\perp e^{-y} X_1\prime(y) + \delta\xi_\perp e^{-y}\left(-\frac{m\Psi}{2\bar{\omega}y} + \frac{\Omega_{i0}^2}{2} + \Psi\right) l_{i1}(y) + \frac{iC\delta\xi_\perp e^{-y}}{2\bar{\omega}}\varphi_{i1}(y),\Big] \tag{16}$$

$$\Omega_{i1}(y) = \frac{1}{\bar{\omega}}\left[m\Psi\frac{l_{i1}(y)}{y} + i(\varphi_{e1}(y) - C\varphi_{i1}(y))\right], \tag{17}$$

$$u_{iz1}(y) = \frac{\sqrt{\delta}F\Psi}{\bar{\omega}} l_{i1}(y). \tag{18}$$

Figure 7 shows the flow vector field at time $t = 0$. As time advances, the mass flow vector field rotates in the clockwise direction, which is the direction of electron diamagnetic drift with B_z into the page. Here, the coordinate x and y label the cross-section of the plasma, with $x = r\cos\theta$ and $y = r\sin\theta$.

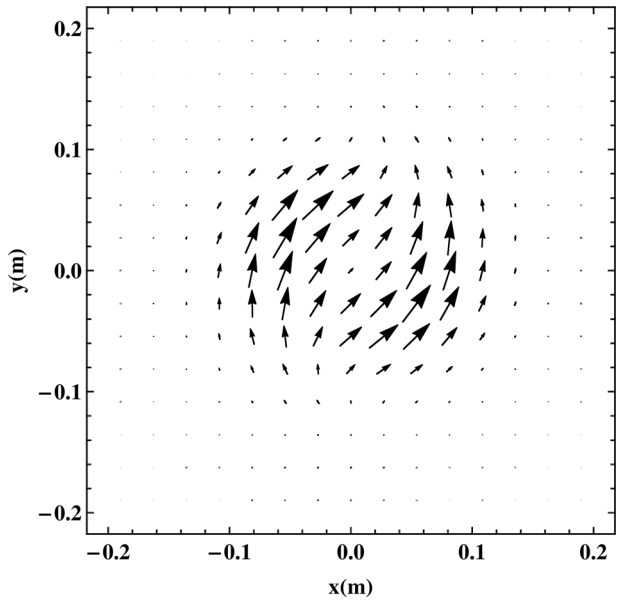

FIG. 7. Vector field plot of the real part of the perturbed mass flow for mode $(m = 1, n = 0)$ in a cross-section of the WOMBAT plasma.

The θ vector points clockwise with z into the page. The mass flow is zero on axis $(x = 0, y = 0)$, consistent with the boundary conditions for density. The symmetric mass flow represents a flow around a stagnant core, with the largest flow in regions of peak density gradient. While we have only studied linear oscillatory response in this work, a similar nonlinear flow pattern may contribute to rotation damping.

V. CONCLUSIONS

In this paper, we employed a two-fluid model, which was developed originally for describing the wave oscillations observed in PCEN,[34,35,43] to study the low frequency oscillations in WOMBAT. To ensure that this model is consistent with WOMBAT, the measured and predicted plasma configurations were compared, including the equilibrium density profile and the space potential profile. These show that although the density and space potential profiles agree, the temperature profile is not flat, as assumed by the model. Next, dispersion curves were generated for WOMBAT plasmas. Compared to the more rapidly rotating centrifuge plasma, the drift wave instability, unstable at larger wavelengths, has a normalized frequency much larger than the normalized frequency for the centrifuge. The difference between dispersion curves is principally due to the low rotation speed of WOMBAT plasmas compared to those of the centrifuge.

Our study of the wave oscillation frequency with B_z and T_e reveals that the measured fluctuation frequency is a factor of 3.5 lower than the predicted frequency, and the predicted trend of oscillation frequency with B_z for inferred T_e matches the data. The discrepancy between the measured and predicted fluctuation frequencies may be attributable to the limitations of assumed temperature uniformity across plasma column. Weaker model limitations may be our neglect of effects induced by plasma fluctuations on the externally applied field. Data limitations include the simultaneous

measurements of plasma rotation profile and probe frequency, and the measured dependency of T_e with B_z.

Finally, we find that the measured and predicted perturbed density profiles have a single peak in the radial direction, indicating the perturbed mode has $n = 0$, and the peak position is in the region of maximum equilibrium density gradient. This qualitative agreement consolidates earlier claims that the mode is a drift mode, driven by the density gradient of the plasma. To our knowledge, this is the first detailed physics model of flowing plasmas in the diffusion region away from the RF source.

[1]N. Rostoker and A. C. Kolb. Phys. Rev. **124**, 965 (1961).
[2]J. P. Freidberg and L. D. Pearlstein, Phys. Fluids **21**, 1207 (1978).
[3]W. A. Perkins and R. F. Post, Phys. Fluids **6**, 1537 (1963).
[4]L. G. Kuo, E. G. Murphy, M. Petravic, and D. R. Sweetman, Phys. Fluids **7**, 988 (1964).
[5]E. B. Hooper, G. A. Hallock, and J. H. Foote, Phys. Fluids **26**, 314 (1983).
[6]R. W. Motley and N. Dangelo, Phys. Fluids **6**, 296 (1963).
[7]M. Krishnan, M. Geva, and J. L. Hirshfield, Phys. Rev. Lett. **46**, 36 (1981).
[8]R. W. Boswell and P. J. Kellogg, Geophys. Res. Lett. **10**, 565 (1983).
[9]R. W. Boswell, S. M. Hamberger, P. J. Kellogg, I. Morey, and R. K. Porteous, Phys. Lett. A **101**, 501 (1984).
[10]A. W. Degeling, T. E. Sheridan, and R. W. Boswell, Phys. Plasmas **6**, 1641 (1999).
[11]F. Greiner, O. Grulke, H. Thomsen, C. Lechte, T. Klinger, and A. Piel, in Proceedings of International Conference on Phenomena in Ionized Gas, Vol. I (Warsaw, Poland, July 11–16, 1999).
[12]X. Sun, C. Biloiu, and E. Scime, Phys. Plasmas **12**, 102105 (2005).
[13]R. W. Boswell and R. K. Porteous, Appl. Phys. Lett. **50**, 1130 (1987).
[14]A. R. Ellingboe and R. W. Boswell, Phys. Plasmas **3**, 2797 (1996).
[15]C. S. Corr and R. W. Boswell, Phys. Plasmas **14**, 122503 (2007).
[16]R. W. Boswell, Plasma Phys. Controlled Fusion **26**, 1147 (1984).
[17]C. Schroder, O. Grulke, T. Klinger, and V. Naulin, Phys. Plasmas **11**, 4249 (2004).
[18]C. Schroder, O. Grulke, T. Klinger, and V. Naulin, Phys. Plasmas **12**, 042103 (2005).
[19]M. Light, F. F. Chen, and P. L. Colestock, Phys. Plasmas **8**, 4675 (2001).
[20]M. Light, F. F. Chen, and P. L. Colestock, Plasma Sources Sci. Technol. **11**, 273 (2002).
[21]A. W. Degeling, T. E. Sheridan, and R. W. Boswell, Phys. Plasmas **6**, 3664 (1999).
[22]R. F. Ellis, E. Mardenmarshall, and R. Majeski, Plasma Phys. Controlled Fusion **22**, 113 (1980).
[23]O. Grulke, S. Ullrich, T. Windisch, and T. Klinger, Plasma Phys. Controlled Fusion **49**, B247 (2007).
[24]W. Horton and J. Liu, Phys. Fluids **27**, 2067 (1984).
[25]O. Sutherland, M. Giles, and R. Boswell, Phys. Rev. Lett. **94**, 205002 (2005).
[26]G. V. Miloshevsky and A. Hassanein, Nucl. Fusion **50**, 1 (2010).
[27]F. F. Chen, *Introduction to Plasma Physics and Controlled Fusion* (Plenum, New York, 1984), Vol. **1**.
[28]H. W. Hendel, T. K. Chu, and P. A. Politzer, Phys. Fluids **11**, 2426 (1968).
[29]M. Okabayashi and V. Arunasalam, Nucl. Fusion **17**, 497 (1977).
[30]H. L. Pecseli, T. Mikkelsen, and S. E. Larsen, Plasma Phys. Controlled Fusion **25**, 1173 (1983).
[31]P. C. Liewer, Nucl. Fusion **25**, 543 (1985).
[32]T. Klinger and A. Piel, Phys. Fluids B **4**, 3990 (1992).
[33]F. M. Poli, S. Brunner, A. Diallo, A. Fasoli, I. Furno, B. Labit, S. H. Muller, G. Plyushchev, and M. Podesta, Phys. Plasmas **13**, 102104 (2006).
[34]M. J. Hole, R. S. Dallaqua, S. W. Simpson, and E. Del Bosco, Phys. Rev. E **65**, 046409 (2002).
[35]M. J. Hole, "Analysis of the rotating plasma column in the vacuum arc centrifuge," Ph.D. thesis (University of Sydney, 2001).
[36]C. S. Corr and R. W. Boswell, Phys. Plasmas **16**, 022308 (2009).
[37]R. W. Boswell, "A study of waves in gaseous plasmas," Ph.D. thesis (Flinders University of South Australia, 1970).
[38]I. A. Biloiu and E. E. Scime, Phys. Plasmas **17**, 113508 (2010).
[39]J. L. Kline, M. M. Balkey, P. A. Keiter, E. E. Scime, A. M. Keesee, X. Sun, R. Hardin, C. Compton, R. F. Boivin, and M. W. Zintl, Phys. Plasmas **10**, 2127 (2003).
[40]E. Scime, R. Hardin, C. Biloiu, A. M. Keesee, and X. Sun, Phys. Plasmas **14,** 043505 (2007).
[41]N. Plihon, C. S. Corr, and P. Chabert, Appl. Phys. Lett. **86**, 091501 (2005).
[42]R. S. Dallaqua, E. Del Bosco, R. P. da Silva, and S. W. Simpson, IEEE Trans. Plasma Sci. **26**, 1044 (1998).
[43]M. J. Hole and S. W. Simpson, J. Phys. D **34**, 3028 (2001).
[44]L. Spitzer, Jr., *Physic of Fully Ionized Gases* (John Wiley & Sons, 1962).
[45]S. Shinohara, N. Matsuoka, and S. Matsuyama, Phys. Plasmas **8**, 1154 (2001).